Probiotics and Antimicrobial Proteins
https://doi.org/10.1007/s12602-025-10486-6

RESEARCH

Bifidobacterium longum Ameliorates Intestinal Inflammation and Metabolic Biomarkers in Mice Fed a High-Fat Diet with Gliadin by Indoleacrylic Acid

Ning Wang[1,2] · Zhangming Pei[1,2] · Hongchao Wang[1,2] · Jianxin Zhao[1,2] · Wenwei Lu[1,2,3]

Accepted: 14 February 2025

Abstract
Gliadin, abundant in flour-based foods and processed foods, has been widely researched for allergies. However, the impact of gliadin on the intestinal barrier of healthy individuals and the intervention effect of *Bifidobacterium longum* (*B. longum*) are rarely explored. Three strains (JCM1217, CCFM1216, CCFM1218) of *B. longum* with strong gliadin hydrolysis were screened from 18 strains. This study explored the effects of *B. longum* on mice with a 10-week high-fat diet and 6% gliadin (HFD + 6%G), assessing duodenal health, lipid metabolism, metabolomics, and gut microbiota in the duodenum and colon changes. Three *B. longum* strains were screened for gliadin hydrolysis to produce minimal R5 immunopeptide production. All three *B. longum* strains improved duodenal morphology, reduced intestinal permeability, reduced inflammation (IL-15), and activated tryptophan metabolism. Additionally, alterations in the microbiota of the duodenum and colon were also observed. Linear discriminant analysis (LDA) showed that the HFD + 6% G group significantly increased the abundance of *Ileibacterium*, *Alistipes*, *Bacteroides*, *Candidatus*, *Saccharimonas*, *Streptococcus*, *Sediminibacterium*, and *Odoribacterium* in the duodenum. The abundance of *Blautia*, *Butyricimonas*, *Ruminococcaceae UCG-010*, *Parabacterioids, and Eubacterium nodatum* in the colon was also increased. The *B. longum* CCFM1216 and *B. longum* CCFM1218 reversed the abundance of these strains. Specifically, *B. longum* CCFM1216 enhanced the duodenal barrier with indoleacrylic acid, beneficial for blood lipids and glucose. These strains may be used as probiotics for gliadin-related diseases.

Keywords Gliadin · High-fat diet · *Bifidobacterium longum* · Indoleacrylic acid · Duodenum

Introduction

Complex peptic ulcer disease [1] threatened the defensive balance of the stomach and duodenum, with global incidence and annual prevalence rates of 0.1–0.19% and 0.12–1.5%, respectively. Duodenal intestinal barrier damage was induced by gastrointestinal diseases, unhealthy diets, and gluten. The causes of duodenal intestinal barrier damage encompassed duodenal ulcer [1], functional dyspepsia [2], Crohn's disease [3], Helicobacter pylori infection [4], nonsteroidal anti-inflammatory drugs [5], and others. Clinical manifestations include increased duodenal mucosal permeability, inflammation, alterations in duodenal gut microbiota, and tissue ulcers. Alcohol [6], coffee, strong tea, genetic variations, and psychological stress can also weaken the duodenal barrier due to excessive stimulation of gastric acid. Gluten primarily causes celiac disease (CD) to the duodenum, with a global prevalence of gluten-related diseases reaching 5%. CD involved the hydrolysis of gliadin [7] into immune peptides in the duodenum, which were presented to pro-inflammatory dendritic cells through immune peptide receptors encoded by HLA-DQ2/HLA-DQ8 genes. The resulting pro-inflammatory factors attack duodenum epithelial cells, leading to villous atrophy and impaired nutrient absorption. Gliadin, a gluten component, is implicated in CD and potentially other conditions like type 1 diabetes, multiple sclerosis, and psoriasis [8], especially among populations consuming large amounts of

✉ Wenwei Lu
luwenwei@jiangnan.edu.cn

1 State Key Laboratory of Food Science and Resources, Jiangnan University, Wuxi, China

2 School of Food Science and Technology, Jiangnan University, Wuxi, China

3 National Engineering Research Center for Functional Food, Jiangnan University, Wuxi, China

Published online: 21 February 2025

refined wheat products and HFD. In China, the prevalence of overweight and obesity among adults was 51% in 2018 [9], and it is projected to reach 65.3% by 2030. Meanwhile, the prevalence of overweight and obesity among school-aged children [10] was 20% in 2018, with a projected increase to 31.8% by 2030. Obesity will become a severe public health issue facing China. HFD promotes the effect of gluten on gluten-tolerant people, while the effect of gluten on healthy people has rarely been explored. Gluten (the main form of gliadin) was found to alter gut microbiota [11], cause obesity [12], and atherosclerosis [13], and exacerbate non-alcoholic fatty liver disease [14]. Compared to a week of normal diet, a gluten-free diet [15] has increased the populations of short-chain fatty acid producers and gut mucosa stabilizers such as *Parabacteroides*, *Barnesiella*, and *Odoribacter*. Based on a study of 242 [16] overweight individuals, refined wheat was less beneficial for weight and body fat reduction compared to high-fiber rye products. Although there was no direct evidence linking obesity to gliadin consumption, both are unfavorable factors for intestinal health.

For duodenal intestinal barrier injury, common therapeutic drugs include drugs that inhibit gastric acid (such as proton pump inhibitors), mucosal protective agents (aluminum phosphate gel), antibiotics (for Helicobacter pylori infection), and drugs that promote gastrointestinal digestion. The most effective treatment for CD [17] is to avoid a containing gluten diet. Currently, there have been no approved drugs for this disease. IMGX-003 [17], AT-1001, and PRV-015 are currently in clinical trials, and their mechanism is gluten endopeptidase, tight junction protein regulator, and monoclonal antibody that binds and inhibits IL-15. However, there may be issues such as over-prescription, adverse reactions, and antibiotic resistance in the drug treatment of duodenal disease injuries. Drug therapy for CD carries the risk of incomplete digestion of gluten leading to the production of immune peptides, which can block anti-tumor risks in refractory CD. Probiotic has the advantages of reducing the pain of patients who mistakenly consume gluten, enhancing intestinal immunity, and improving nutrient absorption.

The mechanisms by which probiotics alleviated CD have been summarized in reviews [18], mainly through toxic peptides' hydrolysis, intestinal barrier protein expression enhancement, and so on. When *B. longum* CECT 7347 [19] intervened in the model of IFN-γ and gliadin sensitization, the strain reduced CD4 +, CD4 +/Foxp3 + cells, and IL-10, and increased CD8 + T cells, indicating that the strain stimulated the CD4 + T cell-mediated immune response. Indole derivatives such as indole-3-acetic acid (IAA) and indole-3-propionic acid (IPA) [20] can enhance the intestinal barrier. The production of indole derivatives [21] by lactic acid bacteria aligned with their predicted metabolic gene rates by over 87%. After screening 960 bacterial species [22] for genes encoding ILA-producing aromatic lactic acid dehydrogenase (ALDH) and tryptophan-synthesizing trpB (FldH homolog), only 95 strains of the Bifidobacterium genus, including 12 *B. longum* strains, possessed both genes. This literature indicated that the *Bifidobacterium* genus has great potential for producing indole derivatives. *B. longum* [23] has alleviated atopic dermatitis symptoms through indole-3-aldehyde or reduced inflammation with IPA [24].

In this study, we hypothesized that *B. longum* can alleviate duodenal harm caused by gliadin in high-fat diet mice, potentially treating gliadin-linked diseases. We evaluated its therapeutic impact on duodenal histology, intestinal permeability, and inflammatory factors. We measured serum metabolites to discover the efficacy foundation for the effectiveness of the strain, and the tryptophan metabolite set was quantified through targeted metabolomics. Mechanistically, *B. longum* repairs duodenal damage via gut microbiota modulation and IA enrichment, as suggested by altered AHR receptor expression.

Materials and Methods

Reagents

The fecal genomic DNA extraction kit was purchased from MP Biomedical Co., Ltd. (CA, USA). The gel recovery kit was purchased from Hangzhou Beiwo Medical Technology Co., Ltd. (Hangzhou, Jiangsu Province, China). The 16S rRNA V3-V4 amplification primers 341F and 806R were purchased from Shanghai Sheng Gong Bioengineering Co., Ltd. (Shanghai, China). The 2 × Taq master mix premix was purchased from Jiangsu Kang Wei Century (Taizhou, Jiangsu Province, China). The mouse TNF-α, IL-15, IL-6, and Zonulin enzyme-linked immunosorbent assay kits were purchased from Shanghai Enzyme Linked Assay Co., Ltd. (Shanghai, China).

Screening of Hydrolytic Gliadin Strains

The trypsin and pepsin-predigested gliadin (PT-gliadin) were prepared according to the *Giorgi* et al.'s method [25]. To assess bacterial hydrolysis of PT-gliadin, we selected 18 strains including *B. longum* (7 strains), *Pediococcusacidilactici* (2 strains), *Clostridium* (4 strains), *Lactobacillus* (4 strains), and *Pseudomonas aeruginosa* (1 strain) in Table S1. All strains were sourced from the Strain Collection Center of the State Key Laboratory of Food Science and Technology at Jiangnan University. After second-generation activation and 12 h of culturing, the bacteria were centrifuged at 4600 g for 10 min and resuspended in sterile PBS to achieve a final concentration of 2×10^9 CFU/mL. Each [26] strain suspension was inoculated into GBM containing 7.5 mg/mL of PT-gliadin at a 3% inoculum rate. The mixer incubated

aerobically at 37 °C and 100 rpm for 48 h. Post-incubation, the mixture was centrifuged at 4600 g for 10 min to obtain fermentation supernatant. For R5 immune peptide detection, the fermentation supernatant was measured as per instructions, and an R5 [27] antibody test was conducted to detect potential peptide toxicity epitope QQPFP.

Design of Animal Experiments

The animal experiment was approved by Jiangnan University's Animal Ethics Committee (JN. NO20230915c1441125 [400]), adhering to Chinese and international animal welfare standards. This modeling method was based on literature [28]. The intervention of a high-fat diet containing 6% gliadin established a model of duodenal injury in mice. Wheat flour contains 9–14% protein, and gluten accounts for 80% of it. Gliadin accounts for about 45% of gluten protein, and gliadin is the main allergen causing wheat allergy. For healthy individuals, long-term intake of wheat flour foods does not seem to cause significant health issues. Gliadin, a gluten component, is implicated in potentially other conditions like type 1 diabetes, multiple sclerosis, and psoriasis [8]. We employed a high-fat diet to amplify the effect of gliadin on the host. The key to the success of this model was the significant increase in body weight of the model mice, along with morphological changes and inflammation in the duodenum.

Nine-week-old male C57BL/6 J mice (SPF grade), weighing 21–25 g, were purchased from Zhejiang Weitong lehua Experimental Animal Technology Co., Ltd. (Beijing, China). These mice were housed in an environment with a temperature of 23 ± 2 °C, humidity of 55 ± 10%, and illumination of 15 ~ 20 LX, accompanied by a 12-h light cycle of day and night. Following a week of acclimatization with ad libitum access to food and water, mice were weighed and balanced into seven groups: NC (normal control), NC + 6% gliadin, HFD (high-fat diet), HFD + 6% gliadin (model), and three models + *B. longum* groups (*B. longum* CCFM1216, *B. longum* CCFM1218, *B. longum* JCM1217), each group with 11 mice (Fig. 2a). The three strains of *B. longum* used in this animal experiment are preserved in the Culture Collection Center of the Food Biotechnology Center at Jiangnan University. The *B. longum* CCFM1218 was isolated from the feces of a 74-year-old male volunteer from Chengmai, Hainan Province. The *B. longum* CCFM1216 was isolated from the feces of a 40-year-old Tibetan female volunteer from the Gairuo Grassl, Sichuan Province. The *B. longum* JCM 1217 standard strain was purchased from the American Tissue Culture Collection. The NC group received standard feed, while NC + 6% gliadin substituted 6% casein with gliadin. Both HFD and HFD + 6% gliadin contained 60% fat, with the latter also substituting 6% casein for gliadin. Detailed feed compositions were in Table S2. The NC and HFD groups were administered PBS solution containing 0.5% cysteine and 1% DMSO orally, while *B. longum* groups received 1×10^9 CFU/mL orally.

The Measurement of Duodenal Morphology and Inflammation Factors

Paraffin-embedded duodenal sections [7] were stained with H&E. Tissue scanning and analysis were performed using digital scanners (Pannoramic MIDI II, 3DHISTECH, Budapest, Hungary) and image Pro Plus (Silver Spring, MD, USA), respectively. The length of the duodenal villi and the depth of the vaginal cavity were analyzed using Image Pro Plus image analysis software.

Biochemical Indicators Determination

The Beckman AU5800 automated biochemical analyzer (Brea, CA, USA) was used to measure serum alanine aminotransferase (ALT), aspartate aminotransferase (AST), triglycerides (TG), total cholesterol (TC), high-density lipoprotein cholesterol (HDL-C), low-density lipoprotein cholesterol (LDL-C) concentrations, C-reactive protein (CRP), and blood glucose (GLU). The levels of tumor necrosis factor – α(TNF-α), interleukin IL-15, IL-6, and Zonulin in the duodenum were detected using an ELISA kit (Shanghai mlBio, Shanghai, China). The content of aromatic hydrocarbon receptors in the duodenum was detected using an ELISA kit (Sbjbio, Nanjing, Jiangsu Province, China).

Characteristics of Gut Microbiota in the Duodenum and Colon [29]

Take an appropriate amount of mouse duodenum stored at –80 °C. Subsequently, employ the Fast DNA Stool Kit (MP Biomedicines, CA, USA) to isolate total DNA from the duodenal tissue. Then amplify the 16 s rDNA V3-V4 region. The V3-V4 regions of the 16 s rDNA were amplified using the forward primer 341F (CCTAYGGGRBGCASCAG) and the reverse primer 806R (GGACTACNNGGGTATCTAAT), with an amplified fragment length of 465 bp. The amplified RNA was recovered and purified using gel recovery reagents, and the recovered amplicons were sequenced using the Illumina Miseq platform (Illumina, Santiago, CA, USA). The steps for measuring fecal DNA samples are the same as those for duodenal operation.

Analysis of Serum Non-targeted Metabolome

The non-targeted metabolomics method for analyzing mouse serum has undergone minor enhancements based on Liao's literature [30]. Simply, the 100 µL of serum was mixed with 3 volumes of pre-cooled methanol, and vortexed for 30 s, meanwhile, the mixture was at – 20 °C for

1 h to precipitate proteins. The mixture was centrifuged at 12,000 rpm for 15 min at 4 °C and was collected 300 µL of the supernatant. Then, the concentrated sample was resuspended in 100 µL of 20% methanol, vortexed again for 30 s, and centrifuged briefly at 12,000 rpm. Finally, the supernatant was collected for analysis. Take an equal volume of samples to make QC for evaluating instrument stability. For the instrument parameter, mobile phase, and data processing related to LC–MS, please refer to our previously published article [31].

Analysis of Tryptophan Metabolites in Feces and Serum

The method for determining the content of tryptophan metabolites in mouse feces and serum is based on literature [24]. In brief, the 50 mg of mouse feces were mixed with 900 µL of 50% methanol, which was homogenized at 65 Hz for 30 s with 10 s intervals, for a total of three cycles. The homogenate was precipitated overnight at 4 °C before being centrifuged at 15,000 g for 10 min. The resulting supernatant was vacuum-concentrated and resuspended in 200 µL of 10% methanol. The resuspended solution underwent centrifugation under the same conditions, and the supernatant was utilized for detection. Mouse serum was blended with methanol in a 1:9 ratio, and the ensuing processing steps were executed by the procedure utilized for mouse feces. The standard substances of tryptophan metabolites were diluted with 10% methanol at 50–0.5 ppm. The mobile phase and detection method utilized were in line with those employed for non-targeted detection in mouse serum.

Statistics Analysis

The experimental data are expressed as mean ± standard deviation (Mean ± SD). Statistical significance was calculated using the R "stats" package. The significance comparison between groups was calculated using a non-paired Wilcoxon test. For all statistical results, # $P<0.05$; # # $P<0.01$; # # # $P<0.001$; Compared with HFD + 6% G, * $P<0.05$; * * $P<0.01$. The non-targeted metabolomics data was integrated into the CD software for comprehensive processing, encompassing deconvolution, normalization, peak extraction, and precise peak alignment. The determination of VIP (variable importance) values for metabolites was performed by the software SIMCA 14.1. The correlation coefficient was calculated employing the "Pearson" method. Furthermore, the predictive pathway analysis of gut microbiota pathways was conducted through the R package "Tax4Fun2" version 1.1.5 [32].

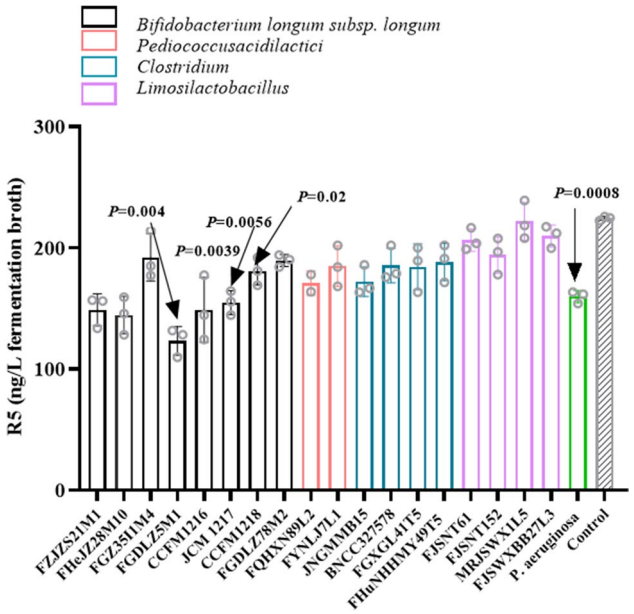

Fig. 1 Immune peptides produced by hydrolysis of PT-gliadin by 18 different types of bacteria. Note: The *P*-value represents a comparison with the control group

Results

Screening of Strains Capable of Hydrolyzing PT Gliadin

Our goal was to identify strains that can hydrolyze PT-gliadin to minimize R5 immune peptides (R5 IPs). The R5 [27] antibody, particularly the 32-mer or 33-mer variant, detects the toxic epitope QQPFP and similar epitopes like QLPYP and PQPFP, which may trigger innate immune responses in CD. Figure 1 shows that among 19 strains from four genera, 8 strains of *B. longum* produced the least R5 IPs. In summary, *B. longum* excels in producing fewer immunogenic peptides from gliadin hydrolysis in vitro. Therefore, we selected 3 strains of *B. longum*, CCFM1216, JCM1217, and CCFM1218 from this species, which exhibited a gradual increase in R5 IP production. And, their capacity will be validated whether to alleviate duodenal barrier damage caused by HFD + 6% G in vivo. While *Pseudomonas aeruginosa* (*P. aeruginosa*) generates little R5 IPs, increased strains are harmful to the duodenal barrier in CD models, as shown by Ren et al. [7].

The Impact of *B. longum* on the Body Weight and Organ Weight of Mice Fed an HFD + 6%gliadin

To amplify the impact of gliadin on the intestinal barrier in mice, a high-fat diet combined with 6% gliadin (HFD + 6% G) was used for modeling. Unless otherwise specified, the

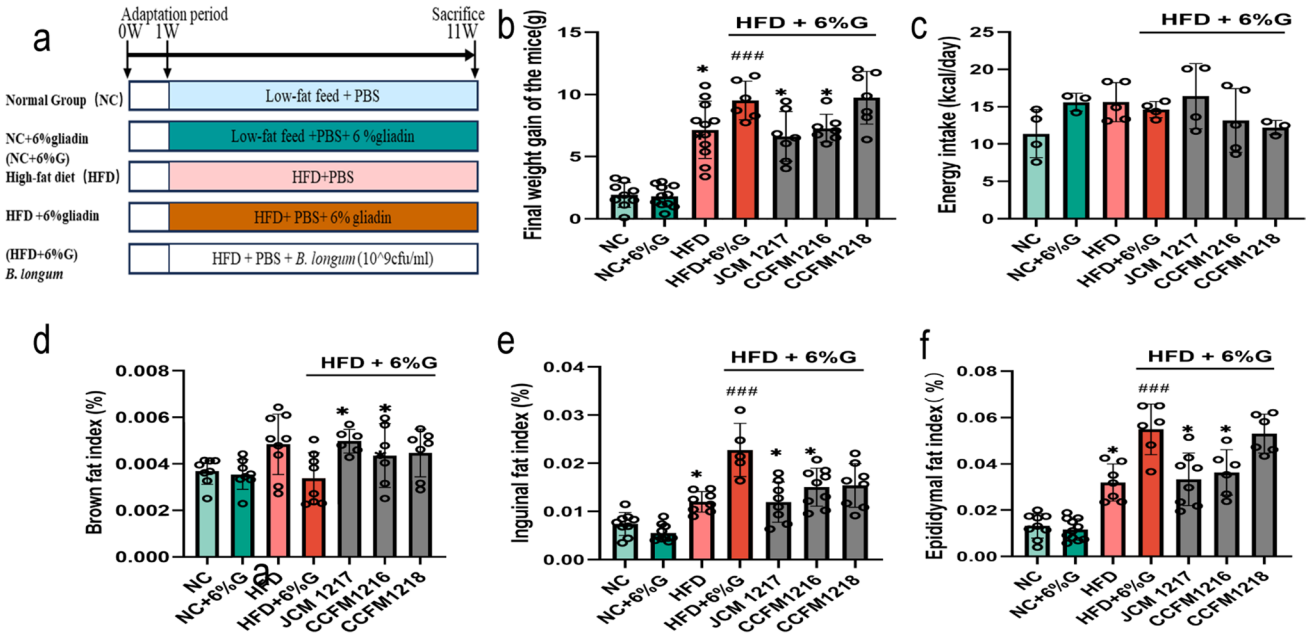

Fig. 2 The effects of *B. longum* on body weight and organ mass in HFD + 6% G mice. **a** Animal experiment design. **b** Weight gain. **c** Energy intake. **d** Brown fat index. **e** Inguinal index. **f** Epididymis fat index. Compared to the NC group, #$P < 0.05$; ##$P < 0.01$; ###$P < 0.001$; compared with HFD + 6% G, *$P < 0.05$; **$P < 0.01$

model group refers to a high-fat diet combined with 6% gliadin. The alleviating effect of three strains of *B. longum* on this model was investigated. As shown in Fig. 2b, after 10 weeks of dietary intervention, the weight of the HFD + 6% G group significantly increased compared with the NC group, indicating successful modeling. Meanwhile, gliadin significantly increased the obesity effect of an HFD. In contrast, *B. longum JCM1217* and *CCFM1216* significantly reduced weight gain compared with the model group. The energy intake of HFD was slightly higher than that of the NC group, and there was no difference in energy intake between the model group and the *B. longum* group (Fig. 2c). In Fig. 2d, in comparison to the model group, the two above-mentioned bacterial strains significantly elevated the brown fat index and conspicuously diminished inguinal fat content (Fig. 2e). This enhancement in brown fat promoted heat generation, subsequently contributing to a reduction in body weight. Notably, only *B. longum* CCFM1216 significantly lowered the epididymal fat index, as illustrated in Fig. 2f. In summary, *both B. longum* JCM1217 *and* CCFM1216 displayed promising effects in facilitating weight loss.

The Impact of *B. longum* on Duodenal Morphology and Inflammation of Mice Fed an HFD + 6%gliadin

Clinically, the pivotal diagnostic criterion for CD[21] is the detection of duodenal morphology. This paper showcased H&E-stained slides of mouse duodenum. As depicted in Fig. 3a, exposure to HFD + 6% G mice resulted in shortened villi, flattened or ruptured villi tips, and enlarged crypts within the duodenum. Consistent with Fig. 3a, b demonstrates a significant reduction ($P < 0.01$) in the villus-to-crypt depth ratio in the model group. Importantly, three strains of *B. longum* exhibited a notable alleviating effect on duodenal pathology, with *B. longu*m CCFM1216 emerging as the most effective strain. Zonulin[22], a pivotal signaling molecule, reversibly modulates intestinal permeability. Our findings indicated that the model group exhibited increased zonulin release (Fig. 3c), suggesting that gliadin exacerbated intestinal permeability in HFD mice. Conversely, *B. longum* CCFM1216 ($P < 0.05$) significantly mitigated zonulin release.

Gluten-degraded peptides in the body [23], particularly α-gliadin p31-43, can elicit innate immune responses by inducing TNF-α and IL-15 production in CD biopsies and fibroblasts, disrupting intracellular vesicle transport involving TLR7. We hypothesized that gliadin's detrimental effects on the intestinal barrier in healthy individuals are linked to these anti-inflammatory factors. Figure 3d–f illustrates that gliadin elevated IL-15 levels in the duodenum of mice under both dietary conditions, whereas *B. longum* CCFM1216 significantly reduces IL-15 production ($P < 0.05$) in mouse duodenum. Although no significant differences were observed in IL-6 and TNF-α levels between the model and *B. longum* groups, a decreasing trend was evident in the intervention group. Given the duodenal morphological damage and the brief 10-week intervention with HFD + 6% G, the moderate alterations

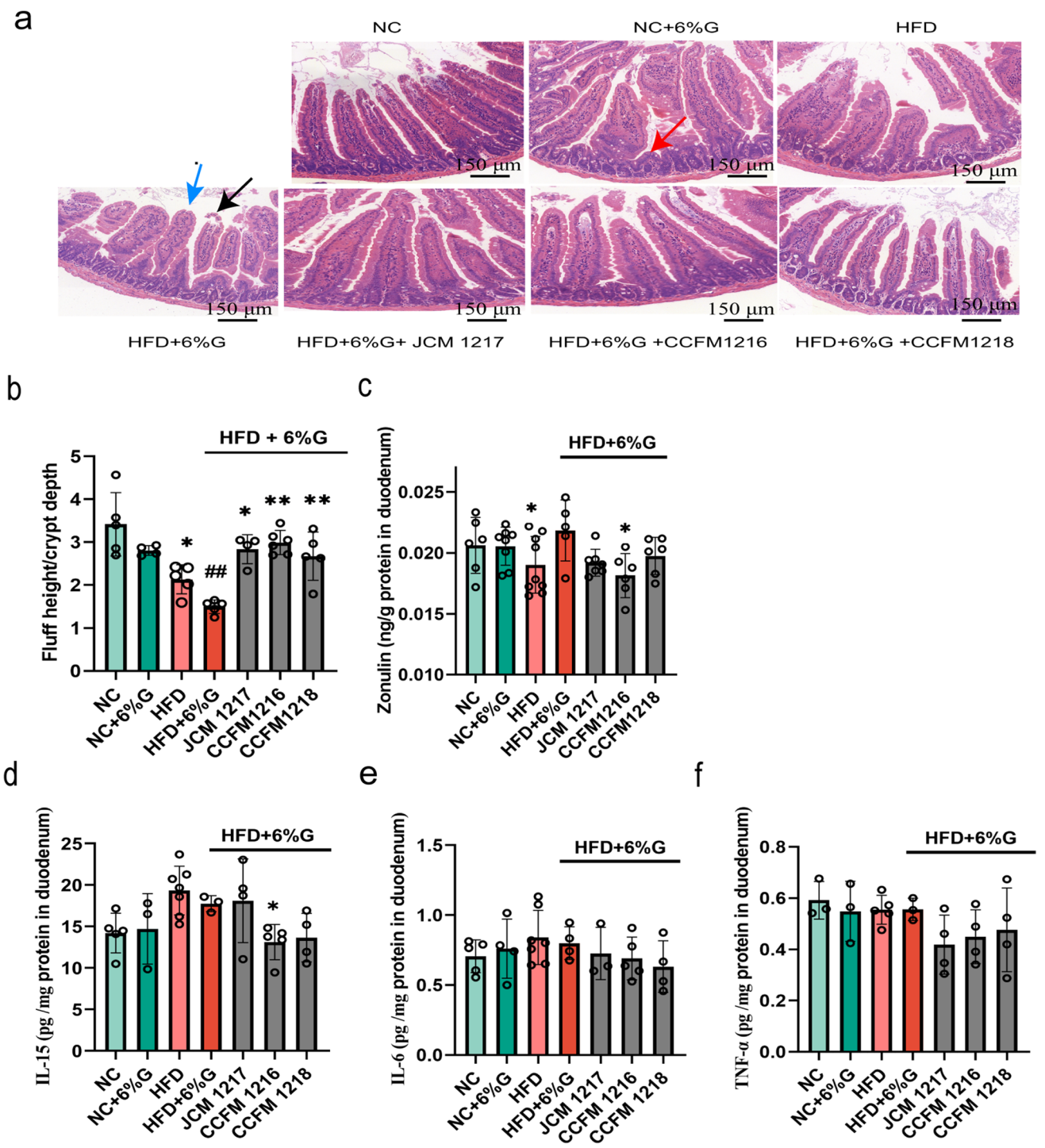

Fig. 3 The effects of *B. longum* on duodenal pathology and inflammation in mice. **a** Duodenal H&E staining (scale: 150 μm, 20×). **b** The ratio of villus length to crypt depth in duodenal. **c** Zonulin content. **d** IL-15 content. **e** IL-6 content. **f** TNF-α content. The blue arrow shows flattened tips of small intestine villi, the black arrow indicates intestinal cell shedding, and the red arrow points to enlarged crypts. Compared to the NC group, #$P<0.05$; ##$P<0.01$; ###$P<0.001$; compared with HFD + 6% G, *$P<0.05$; **$P<0.01$

in inflammatory markers likely stem from them. Additionally, in healthy individuals, we speculated that the duodenal damage induced by gliadin is likely to be mild and progressive.

The Impact of *B. longum* on Blood Biochemical Indicators of Mice Fed an HFD + 6%gliadin

An HFD is often correlated with disruptions in blood lipid,

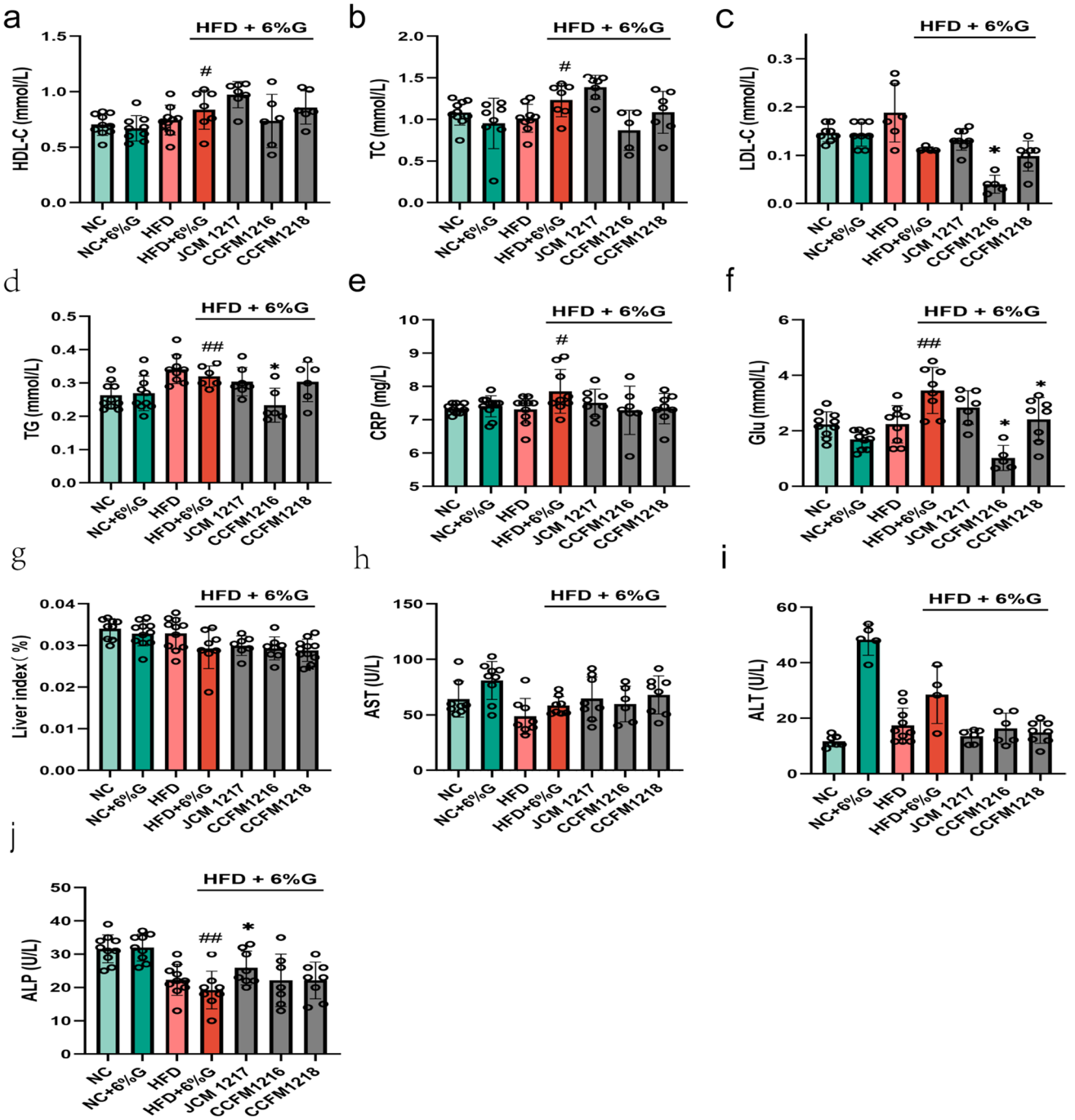

Fig. 4 The effect of *B. longum* on blood lipids and liver function in mice. **a** High density lipoprotein cholesterol, total cholesterol;(HDL-C, TC). **b** Low density lipoprotein cholesterol, Triglycerides; LDL-C, TG. **c** C-reactive protein (CRP). **d** Blood sugar. **e** Liver index. **f** Alanine aminotransferase (AST). **g** Aspartate transaminase (ALT). **h** Alkaline phosphatase (ALP); compared to the NC group, #$P<0.05$; ##$P<0.01$; compared with HFD + 6% G, *$P<0.05$; **$P<0.01$

glucose metabolism, and weight. Figure 4a and b demonstrates elevated blood lipid markers in the model group compared to NC, while *B. longum* CCFM1216 showed superior lipid-lowering effects. CRP [24], an acute-phase protein indicative of inflammation or tissue damage, was significantly elevated in the model group (Fig. 4d), mirroring duodenal tissue damage. Additionally, the model group experienced heightened blood glucose, which was effectively mitigated by *B. longum* CCFM1216 and *B. longum* CCFM1218, underscoring *B. longum*'s capacity to regulate glucose metabolism in an HFD.

We aimed to explore the impacts of gliadin on liver function. Figure 4e highlights a notable reduction in liver index in the HFD + 6%G model group versus the NC group, suggesting gliadin's role in lessening liver fat accumulation. However, Fig. 4f–h reveals no signs of liver dysfunction despite this decrease, and both the model and intervention groups exhibited similar liver function to the NC group.

The Impact of *B. longum* on the Serum Untargeted Metabolome of Mice Fed an HFD + 6%gliadin

Figure 5a and b showcases distinct metabolite profiles among groups (PERMANOVA $P < 0.01$). In positive ion mode, R2x, R2y, and Q2 were 1 and 0.9, respectively. For negative ion mode, respective scores were 0.922, 1, and 0.946, confirming high model reliability (Fig. S1). R2 gauges fit, while Q2 assesses predictive capacity post-validation. Model validation through 200 permutations yields R2 and Q2 values of 0.992 and − 0.0904 in positive mode and 0.98 and − 0.572 in negative mode (Fig. S2). In both modes, the Q2 regression line's y-axis intersection is negative, suggesting no overfitting. After BH correction, significant metabolites ($P < 0.05$, fold change < 0.8 or ≥ 1.25) were filtered between *B. longum* CCFM1216 and HFD + 6% G groups, yielding 31 differential metabolites. Of these, 21 were upregulated and 10 downregulated in *B. longum* CCFM1216, compared to HFD + 6% G.

Using the MetaboAnalyst platform to analyze the differences in metabolites between the *B. longum* CCFM1216 group and model group, enrichment analysis revealed that phosphatidylcholine biosynthesis, histidine metabolism, and methionine metabolite sets were more enriched (Fig. 5c). The pathway of metabolites products focused on pathways such as alanine metabolism, histidine metabolism, aspartate metabolism, and methionine metabolism (Fig. 5d). Enrichment and pathway analysis share the same changes in metabolite sets, such as arginine and proline metabolism, histidine metabolism, tryptophan metabolism, and methionine metabolism. Gliadin is a protein complex, and its degradation process inevitably involves amino acid metabolism. Tryptophan metabolism [33] and methionine metabolism [34] may be key pathways for the *B. longum* CCFM1216 group to alleviate intestinal barrier damage in HFD + 6% G group mice.

Thirty biomarkers were screened through enrichment analysis and pathway analysis. Figure 5e compares their levels in a model group and three *B. longum* strains. Compared to HFD + 6%G, tryptophan, IA, and Indole aldehyde (IAld) were enriched in *B. longum*, aligning with prior pathway analyses. The serum untargeted metabolomics analysis illustrated that (Fig. 5), The *B. longum* groups also showed higher content of methionine, and proline, suggesting enhanced gluten degradation.

The Effect of *B. longum* on Tryptophan Metabolism in Feces and Serum of Mice Fed an HFD + 6%gliadin

Untargeted metabolomics indicated that tryptophan-derived indole derivatives may be key substances for *B. longum* CCFM1216 to alleviate model damage. Tryptophan metabolism, including kynurenine, 5-HTP, and indole pathways, occurs in the liver and gut microbiota. Gut microbiota produces indole derivatives, beneficial for gut immunity and inflammation. To elucidate whether the tryptophan metabolites' variations between the above groups stem from the gut microbiota, we conducted a quantification of these metabolite levels in both mouse feces and serum samples. In Fig. 6, compared with HFD + 6% G, the three strains of *B. longum* can increase the content of IA, indole-3-acetic acid (IAA), and indole-3-lactic acid (ILA) in feces, while IA showed significant differences in the intervention group (Fig. 6c). Compared to the model group, *B. longum* CCFM1216 exhibited the greatest increase in the expression of duodenal aromatic hydrocarbon receptors (AHR, $P = 0.057$, Fig. 6f).

In mice serum (Fig. S3 3a-3b), three strains of *B. longum* significantly increased the IA content, yet there was no significant difference in tryptophan content among the groups. The indole-3-carboxaldehyde (IAld, Fig. S3 3c-3d) was detected with no significant differences among groups. However, we only detected these three tryptophan-related metabolites in the serum, and the reason probably is that these substances are mainly degraded by gut microbiota and enriched in the intestine. Notably, *B. longum* CCFM1216 increased the content of IA in mice serum and feces, enhancing the gut barrier (Figs. 6c and S3 3b). Compared to the model group, *B. longum* CCFM1216 significantly increased the content of IA and Ahr.

The Effect of *B. longum* on Duodenal Microbiota of Mice Fed an HFD + 6%gliadin

Gliadin digestion [35] and absorption primarily occur in the duodenum, emphasizing the crucial role of gut microbiota. Research indicated probiotics alleviate gliadin-induced intestinal damage by modulating microbiota composition [25, 36]. This study employed 16 s rRNA amplicon sequencing to assess *B. longum* strains' impact on duodenal microbiota structure in mice fed with an HFD + 6% gliadin. Alpha diversity represents intra-group species richness and evenness (e.g., Shannon index, observed species). Beta diversity, via PCoA based on Bray–Curtis distances, captures intergroup variations. Figure 7a and b reveals that HFD + 6% gliadin reduced species diversity but not evenness, while *B. longum* strains restored species number without altering evenness. Figure 7c demonstrates *B. longum* CCFM1216 effectively reversed HFD + 6% gliadin-induced microbiota

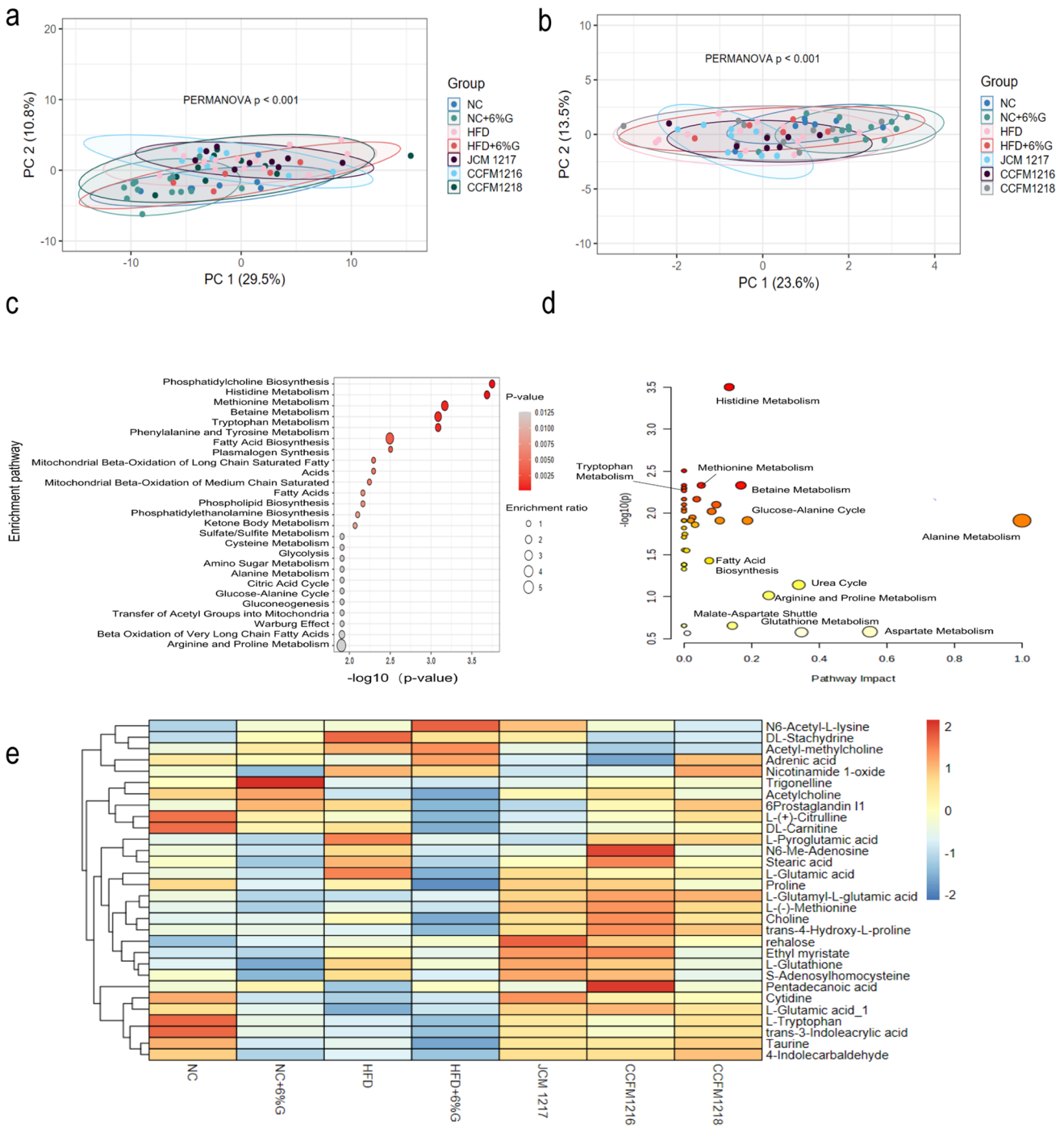

Fig. 5 Enrichment and pathway analysis of differential metabolites in the serum of mice from the *B. longum* CCFM1216 and HFD + 6%G groups. **a** Metabolites in C18 positive ion mode. **b** Metabolites in C18 negative ion mode. **c** Enrichment analysis of differential metabolites. **d** Pathway analysis differential metabolites. **e** Comparison of differential metabolites in mouse serum. The color of each cell in the heatmap represents the average relative metabolite content in the serum of each group's mice, with deeper orange indicating higher values and deeper blue indicating lower values. Compared to the NC group, #$P < 0.05$; ##$P < 0.01$; compared with HFD + 6% G, *$P < 0.05$; **$P < 0.01$; non paired Wilcoxon test is used to calculate P-values

alterations, with similar trends observed for the other two *B. longum* strains.

LDA was utilized to dissect the genus-level differences across groups. This study selected the NC group, the HFD + 6% G group, and three intervention *B. longum* strains,

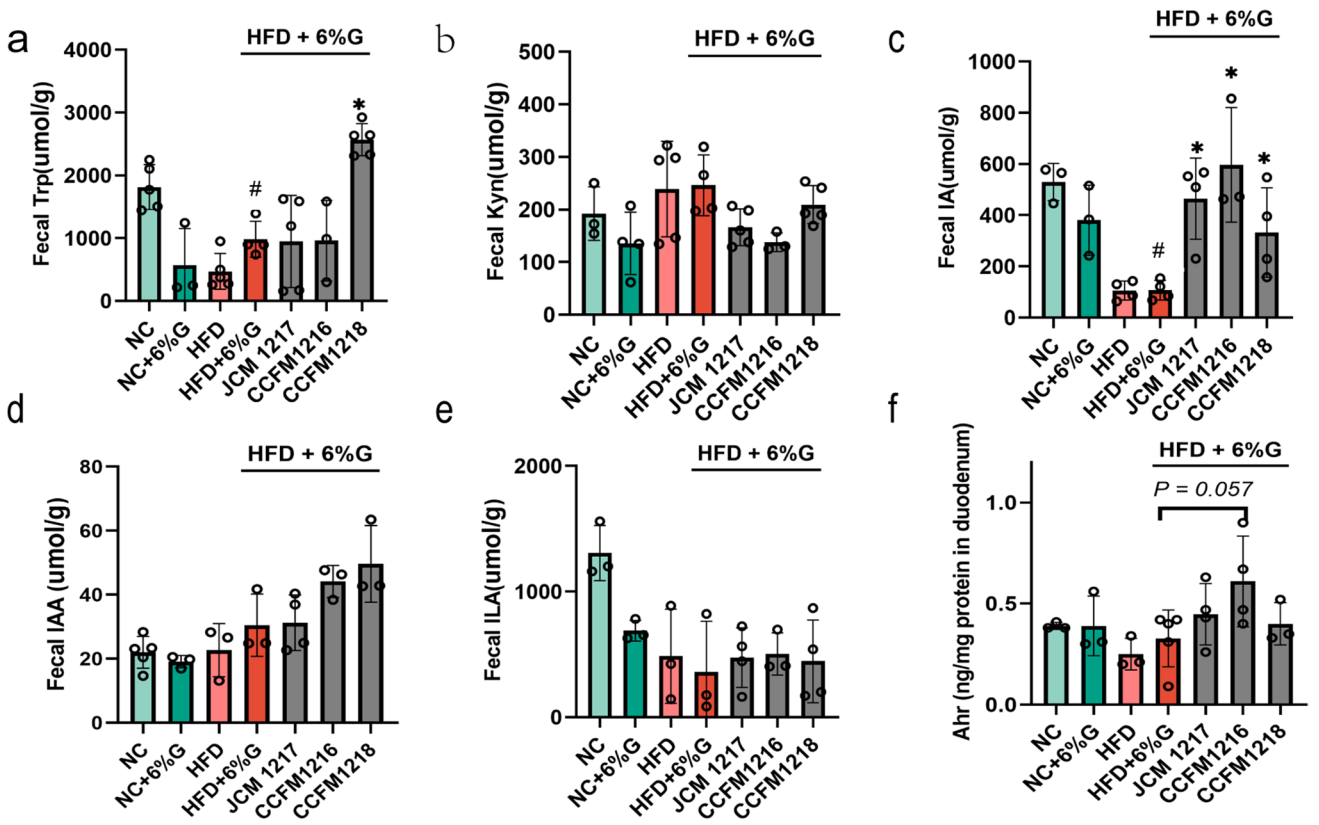

Fig. 6 Analysis of tryptophan metabolites in mouse feces. Note: **a** Tryptophan (Trp); **b** Kynurenine (Kyn); **c** Indoleacrylic acid (IA); **d** indole-3-acetic acid (IAA); **e** Indole lactic acid (ILA); **f** Aryl hydrocarbon receptor (Ahr) (compared with HFD + 6% gliadin group, $*P < 0.05$, $**P < 0.01$)

aiming to elucidate the therapeutic potential of intervention groups against the HFD + 6% G challenge. By applying thresholds of LDA scores < 2 and alpha values < 0.05, comprehensive identification of 21 distinct genera was achieved, as depicted in Fig. 7D. In contrast to the NC group (Fig. 7e), the HFD + 6% G group exhibited a significant enrichment of genera such as *Ileibacterium*, *Alistipes*, *Bacteroides*, *Candidatus, Saccharimonas*, *Streptococcus*, *Sediminibacterium*, and *Odoribacterium*. Notably, the *B. longum* CCFM1216 and CCFM1218 effectively mitigated the abundance of these taxa. Meanwhile, the above two *B. longums* fostered the proliferation of *Faecalibaculum*, *Acinetobacter*, *Peredibacter*, *Clostridium*, *Pseudochromobutrum*, and *Adlercreutzia*.

Alterations in gut microbiota composition can modulate its metabolic activity. We employed 16S rRNA gene sequencing and the Tax4Fun2 [32] R package, by the KEGG pathway, to explore the functional shifts in gut microbiota post-intervention with *B. longum*. In Fig. 7f and g, compared to the NC group, the model group displayed reduced biosynthesis of phenylalanine, tyrosine, tryptophan, biosynthesis of secondary metabolites, pantothenate, and Pantothenate and CoA biosynthesis. Meanwhile, the model group enhanced glutathione metabolism, biofilm formation — Vibrio cholerae, cyanoamino acid metabolism, steroid biosynthesis, and primary bile acid biosynthesis. Notably, the *B. longum* JCM 1217 and *B. longum* CCFM1216 partially restored these metabolic pathways, aligning closer to the NC group.

The Effect of *B. longum* on Colonic Microbiota of Mice Fed an HFD + 6%gliadin

The median time [37] that food is spent in the large intestine of healthy individuals was 21 h. After passing the stomach and small intestine, undigested gliadin fragments escape to the colon, where colonic microorganisms metabolize them. We utilized 16 s rRNA amplicon sequencing to assess how 3 strains of *B. longum* affect the colon microbiome of mice. Figure 8a reveals that 6% gliadin increases microbial species regardless of diet type, enhancing diversity without affecting evenness. Figure 8b shows that HFD + 6%G did not alter the colon Shannon index. The *B. longum* group did not significantly impact the Shannon index or species count, suggesting a limited influence on intra-group diversity. Figure 8c indicates sectional genus differences between NC and HFD + 6%G groups, but the *B. longum* partially restored the

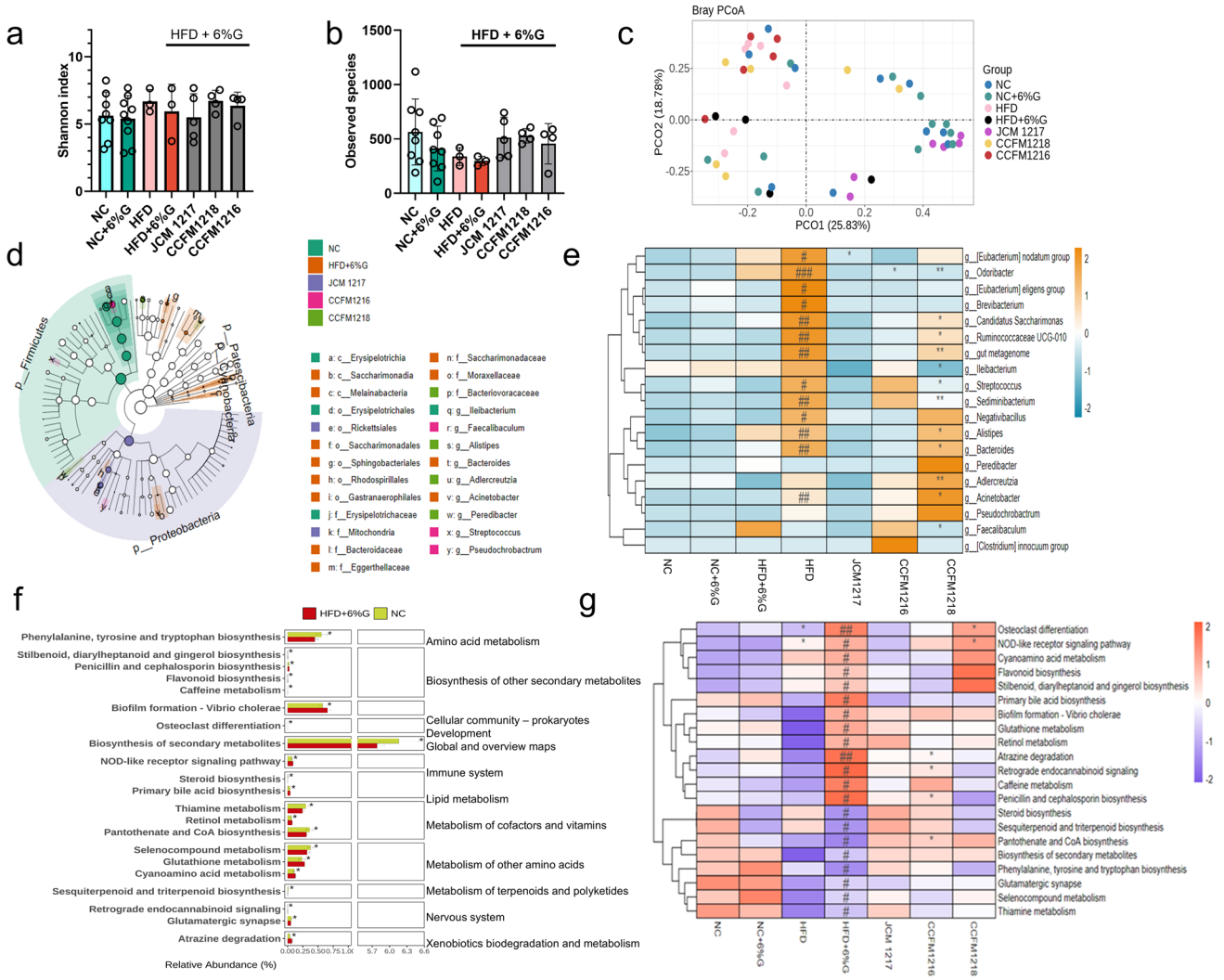

Fig. 7 The effect of *B. longum* on the gut microbiota in the duodenum of mice. **a** Shannon index. **b** Observed species. **c** Principal coordinates analysis (PCoA). **d** Cladogram depicting the differentially abundant taxa (LDA score > 2 and $P < 0.05$) among groups. **e** Distribution of remarkably changed genes among groups. The color of each cell in the heatmap represents the mean relative abundance of each genus in the duodenum of each group's mice, with deeper yellow indicating higher values and deeper cyan indicating lower values. **f** Differential metabolic pathways between NC and HFD + 6% G group. **g** Distribution of remarkably changed functional metabolic pathway among groups. The color of each cell in another heatmap represents the mean relative abundance of predicted functional pathways of duodenal microorganisms in each group's mice, with deeper orange indicating higher values and deeper blue indicating lower values; Compared with the NC group, #$P < 0.05$, ##$P < 0.01$; compared with the HFD + 6% gliadin group, *$P < 0.05$, **$P < 0.01$. Non paired Wilcoxon test is used to calculate *P*-values

model's microbiota, showing minimal overall structural differences between intervention and model groups.

LEfSe was employed to compare bacterial genus differences in the colon. This study selected the NC group, HFD + 6%G, and 3 strains of *B. longum* groups to evaluate *B. longum's* therapeutic effects. Applying LDA > 2 and alpha < 0.05 thresholds, 23 distinct species were identified (Fig. 8d). Compared to NC (Fig. 8e), the group HFD + 6%G boosted *Blautia*, *Butyricimonas*, *Ruminococcaceae UCG-010*, *Parabacterioids*, *and Eubacteria nodatum*, while reducing *Escherichia Shigella* and *Bifidobacterium*. Notably, *B. longum* CCFM1216 and CCFM1218 reversed these shifts.

Alterations in gut microbiota can impact its metabolic functions, thereby affecting the host's metabolism. We used 16S rRNA gene sequencing and Tax4Fun2 R package to study gut microbiota function changes post-*B. longum* intervention. Figures 8f and S4 depict distinct metabolic pathways altered in HFD + 6%G and all groups, respectively. Compared with the normal diet, only the microbial pathways significantly changed in the HFD + 6% G group, and we suspected that these species were more closely related

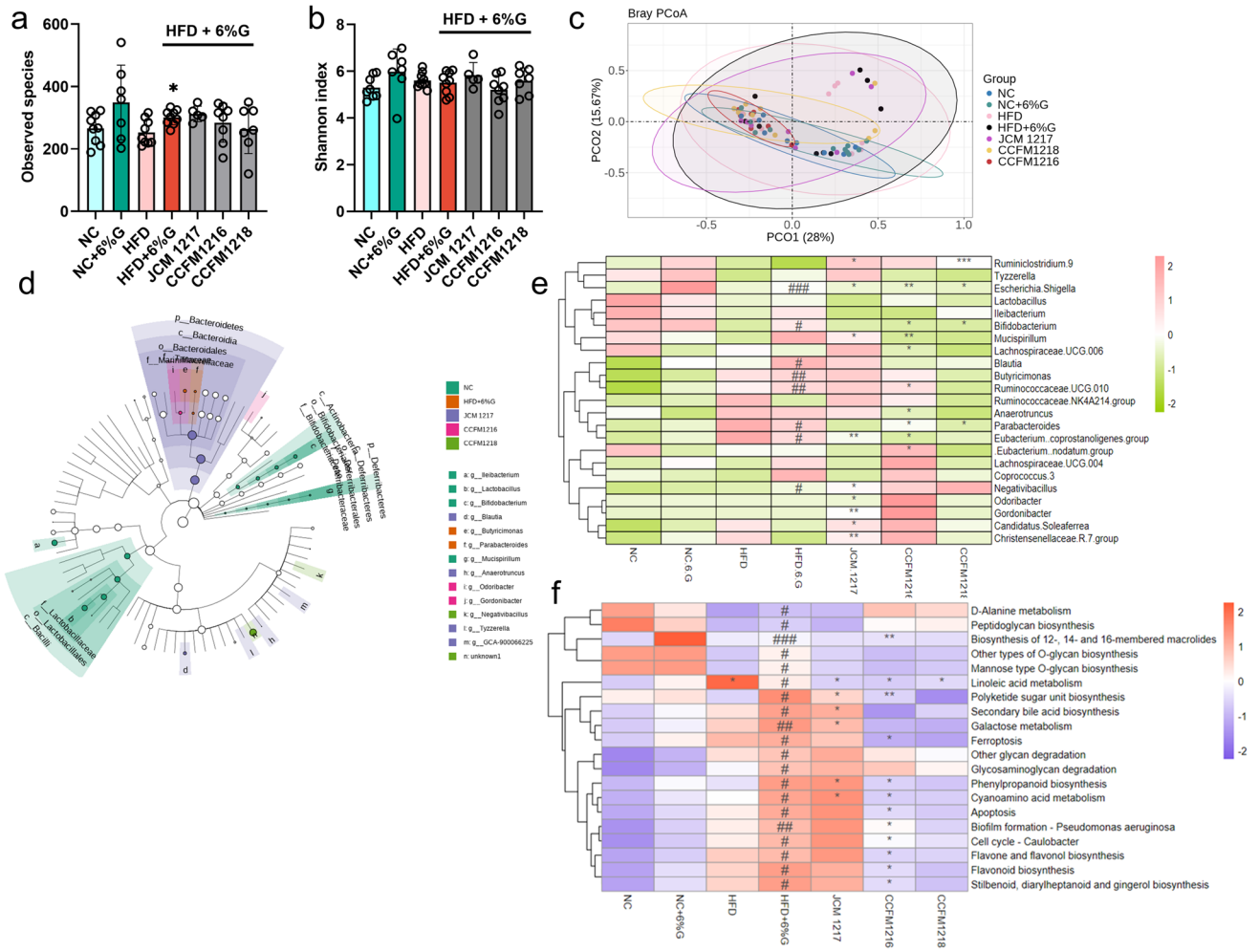

Fig. 8 The effect of *B. longum* on the gut microbiota in the colon of mice. **a** Shannon index. **b** Observed species. **c** Principal co-ordinates analysis (PCoA). **d** Cladogram depicting the differentially abundant taxa (LDA score > 2 and $P < 0.05$) among groups. **e** Distribution of remarkably changed genus among groups. The color of each cell in the heatmap represents the mean relative abundance of each genus in the colon of each group's mice, with deeper red indicating higher values and deeper green indicating lower values. **f** Differential metabolic pathways between NC and HFD + 6% G group. **g** Distribution of remarkably changed functional metabolic pathway among groups. The color of each cell in the heatmap represents the mean relative abundance of each genus in the colon of each group's mice, with deeper orange indicating higher values and deeper purple indicating lower values; Compared with the NC group, #$P < 0.05$, ##$P < 0.01$; compared with the HFD + 6% gliadin group, *$P < 0.05$, **$P < 0.01$. Non paired Wilcoxon test is used to calculate *P*-values

to HFD (Fig. 8f). The model group showed reduced D-Alanine metabolism, peptidoglycan biosynthesis, Mannose type O-glycan biosynthesis, and Linoleic acid metabolism. Meanwhile, the model group increased biofilm formation-*Pseudomonas aeruginosa*, apoptosis, secondary bile acid biosynthesis, and Flavone and flavanol biosynthesis, and *B. longum* CCFM1218 and *B. longum* CCFM1216 partially restored these pathways to NC levels. Adding gliadin to HFD significantly reduced linoleic acid metabolism, indicating a shift towards gliadin metabolism. In Fig. S5, the model group significantly increased the two-component system and carbon metabolism of colonic microorganisms, while significantly decreasing ABC transporters, Quorum sensing, and other predicted functional pathways. Further metagenomic sequencing is needed to understand gliadin-related microbial functional changes.

Correlation Analysis Between Gut Microbiota and Multiple Indicators

A correlation analysis was performed on the changed microbiota in the duodenum and colon, along with the ratio of villus length/crypt depth in the duodenum, the fecal targeted metabolites, and inflammatory factors. In Fig. S6, *Lactobacillus* in the duodenum ($P < 0.05$) was positively correlated with fecal IA, while *Eubacterium coprostanoligenes* in the duodenum ($P < 0.01$) was negatively correlated with this substance. The *Christensenellaceae* in the duodenum

was positively correlated with villus length/crypt depth ($P < 0.01$). *Ruminococcaceae* ($P < 0.01$) showed a remarkable negative correlation with the inflammatory factor IL-15 in the duodenum.

Based on the correlation analysis among the villus-to-crypt depth ratio, inflammatory factors, changes in gut microbiota, and serum and fecal metabolites. There is a correlation between more than one small intestine and colon microbiota and a single metabolite and biochemical indicator, indicating that *B. longum* alleviates duodenal inflammation by regulating gut microbiota, and then modulating metabolite changes. Specifically, *Lactobacillus* and IA are positively correlated (Fig. S6). In short, we conjectured that *B. longum* CCFM1216 improved *Lactobacillus* in the gut, raising IA levels and reducing duodenal damage.

Discussion

The human gut [38] contains around 10^14 microorganisms, playing a crucial role in food digestion and maintaining gut immunity. Some research [39] showed that probiotics like *Bifidobacteria* can reduce intestinal harm in CD patients caused by gliadin. For healthy people, published literature showed that gliadin has a certain relationship with human intestinal microorganisms [40], diabetes [41], and so on. Among 18 bacterial strains, *B. longum* produced the least amount of immunopeptides for the hydrolysis of PT-gliadin. Hence, we investigated the therapeutic potential of three *B. longum* strains on the duodenum of HFD + 6% gliadin mice. Our findings suggested that *B. longum CCFM1216* effectively mitigated duodenal barrier damage induced by gliadin.

We first examined the effects of *B. longum* on biochemical indicators and duodenal inflammation in the model group. Rune et al. [42] investigated the impact of adding 1% gliadin to a high-fat diet of Apoe -/- mice over 16 weeks. Variations in microbial composition were observed, yet glucose tolerance, insulin levels, and blood lipids remained unchanged. This is consistent with our results, where the addition of gliadin increased the levels of blood lipids and blood glucose, but not significantly. However, the amount of gliadin added and the method of blood glucose measurement were different in the two studies. In this study, an HFD exacerbated gliadin's disruption of duodenal morphology and increased intestinal permeability, consistent with literature reports [7]. Remarkably, *B. longum* CCFM1216 effectively lowered LDL-C, TG, and blood glucose levels (see Fig. 4). Beyond disrupting duodenal morphology, gliadin may also perturb intestinal mucosal immunity. In CD [7] pathogenesis, gluten peptides traversed the duodenum, stimulating dendritic cells to present antigens to T cells, triggering IL-15 secretion and subsequent attacks on intestinal epithelial cells. *Przemioslo* et al. [43] reported heightened IL-6 and TNF-α production in the lamina propria and epithelium of untreated CD patients' small intestines, compared to healthy individuals. Notably, TNF-α contributed to duodenal mucosa damage in CD and acted as a systemic inflammatory mediator [43]. Children who developed CD by age 6 ($N = 56$) exhibited heightened IL-6 production during at initial 4 months before gluten introduction, compared to the healthy children ($N = 27$) [44]. Our experimental model showed increased inflammatory factor release in the duodenum of the model group, suggesting a persistent yet subtle impact of gliadin on healthy duodenal tissue. We hypothesize that in healthy individuals, gliadin may induce mild duodenal damage.

Targeted and untargeted metabolomics provided valuable insights into the beneficial effects of the *B. longum*. The serum untargeted metabolomics indicated that (Fig. 5) the *B. longum* groups also showed higher content of methionine, and proline, suggesting enhanced gluten degradation. The *B. longum* has gluten-degrading potential [45, 46]. The targeted analysis indicated that tryptophan, IA, IAld, and IAA were enriched in the feces of mice treated with *B. longum* (Fig. 6). Literature [47] noted Indole acrylic acid's role in treating inflammatory bowel disease. Gliadin increased small intestine permeability, while tryptophan metabolites from microorganisms, such as ILA, indole-propionic acid [20], and indole-3-acetate, could repair intestinal structure [48] and strengthen the barrier via AHR. Thus, we speculated that *B. longum CCFM1216* enhanced the duodenal barrier by degrading gluten and producing high levels of indole compounds.

Gliadin digestion and absorption primarily occur in the duodenum, which is also the immune focus for CD. We reasonably speculated that gliadin will cause different microbial characteristics of the duodenum compared to the NC group. We have summarized some literature on bacterial genera with significant changes in the duodenum. Literature [49, 50] reported that *Bacteroides*, *Streptococcus, Odoribacter, Clostridium*, *Bifidobacterium*, and *Lactobacillus* are responsible for gliadin degradation. Interestingly, *Adlercreutzia* [51], though associated with high-fat soybean oil diets, does not participate in gliadin metabolism. The proliferation of *Alistipes* in the model group was found to contribute to intestinal tryptophan degradation, whereas *B. longum JCM 1217 and B. longum CCFM1216*, by modulating the gut microbiota, mitigated this effect, enhancing tryptophan metabolism and thereby safeguarding the intestinal barrier. From this study and pertinent literature [52], the potential of the harmless group *Clostridium* as a microbial biomarker that inhibited CD. In the future, this genus will act as a probiotic candidate for the therapeutic of CD.

In healthy individuals, food has a median residence time of 21 h as it passes through the upper gastrointestinal tract to the large intestine [37]. Undigested gliadin fragments that escape the stomach and small intestine reach the colon,

where colonic microorganisms metabolize these short peptides. Rune et al. [42] found that adding 1% gliadin did not significantly alter the PCoA clustering of fecal microbiota from an HFD. This paper presented partial overlap between the NC group and the model group (Fig. 8c) indicating that gliadin has little effect on colonic microbiota. Reference [53] indicated that *Butyricimonas* were more abundant in media containing digested gluten, and the subspecies *Butyricimonas* spp. could improve indicators such as weight, blood glucose levels, and insulin resistance in HFD. This genus of bacteria is enriched in both *B. longum JCM 1217* and *CCFM1216*. *Blautia* and *Ruminococcaceae* increased in the dietary pattern with the addition of 6% gliadin, while decreasing in the intervention groups with *B. longum*. Consistent with the literature [54], the abundance of *Blautia* and *Ruminococcaceae* decreased after treatment with *Bacillus subtilis LZU-GM*, a probiotic that can degrade gluten in vitro. This genus of strain, *Ruminococcus caceae UCG-013* [55], was positively correlated with HDL-C levels in obese mouse serum and negatively correlated with serum TC, TG, and LDL-C levels and has been identified as a microbial indicator of obesity prevention. Previous literature [56] has shown that Bifidobacterium decreased in high-fat diets, which was consistent with the results of the model group in this study. The low content of *B. longum* in the intervention group may be due to the low colonization efficiency of the intervention strain. The reason is that [57] gluten (84.5%) strongly inhibited the single biofilm of *Lactobacillus rhamnosus*, which meant that probiotics were not easily adhered in the gastrointestinal tract where gluten was present. Interestingly, adding gliadin to a normal diet did not significantly increase the abundance of *Escherichia Shigella*, while adding gliadin to an HFD significantly reduced the abundance of the genus (Fig. 8e). Xie et al. [58] demonstrated that adding gluten to BALB/c mice (intramuscular injection of 0.5 mg gluten for 21 days, gavage of 10 mg for 14 days) also enriched *Escherichia Shigella*, which was a marker of obesity in the small intestinal microbiota in HFD [58, 59]. The microbiota in the model group, capable of breaking down gliadin, seems to mitigate the harmful effects of HFD. In short, the three strains of *B. longum* lead to distinct microbial patterns distinct from the model.

Among gut microbes, *Ileibacterium*, *Odolibacterium*, and *Negativibacillus* coexist in feces and small intestine. *Ileibacterium* remained stable across sites and groups. In the duodenum, *Odoribacter* increased in the model group but reduced in *B. longum CCFM1216*. Conversely, in feces, it is stable in the model but raised in *B. longum CCFM1216*. The *Odoribacter* [60] positively correlated with gluten-free diet adherence in celiac patients. This strain was responsible for producing butyric acid in the colon, and its significant increase in feces may represent the intestinal mucosa's integrity. *Negativibacillus* surged in the model group (duodenum and feces) vs. NC, staying high in *B. longum CCFM1216*. The strain significantly increased in ulcerative colitis, indicating that the model group may have intestinal inflammation, while the intervention group reduced this adverse effect.

In Fig. S6, based on the correlation analysis among the villus-to-crypt depth ratio, inflammatory factors, changes in gut microbiota, and serum and fecal metabolites. There is a correlation between more than one small intestine and colon microbiota and a single metabolite and biochemical indicator, indicating that *B. longum* alleviates duodenal inflammation by regulating gut microbiota, and then modulating metabolite changes. Among them, serum metabolomics and microbial functional analysis jointly target indole compounds involved in tryptophan metabolism, especially IA.

However, this study still has limitations. Firstly, metagenomic techniques should be employed to identify changes in species related to the duodenum and colon that are both involved in gliadin hydrolysis. Secondly, the molecular mechanism by which *B. longum* CCFM1216 alleviates duodenal inflammation remains unclear and may be investigated in future studies. Lastly, a purer model should be considered to simulate the effects of gliadin on healthy individuals, rather than under high-fat diet conditions.

Conclusions

This study investigated the effects of three strains of *B. longum* on the morphology of the duodenum, serum untargeted metabolome, fecal targeted tryptophan, and changes in duodenum and colon microbiota in HFD + 6% gliadin mice. The results showed that *B. longum* CCFM1218 and *B. longum* CCFM1216 enhanced the intestinal barrier, alleviated duodenal injury, and reduced intestinal permeability by regulating the microbial community of the duodenum and colon. In summary, these two strains of *B. longum* enhance gliadin hydrolysis and modulate intestinal microbiota to enrich the content of IA, IAA, and ILA, thereby mitigating gliadin's impact on intestinal barrier function. Among them, *B. longum* CCFM1216 modulates the gut microbiota, particularly by regulating lactobacilli, to enhance the levels of IA and Ahr, thereby promoting healthy blood lipid and blood glucose metabolism. This study provides a foundation for exploring the impact of gliadin on individuals with obesity tendencies and for developing probiotic resources that regulate gliadin's effects on intestinal barriers.

Supplementary Information The online version contains supplementary material available at https://doi.org/10.1007/s12602-025-10486-6.

Acknowledgements We thank all participants and researchers of this study.

Author Contributions Conceptualization, N. W. and W. L.; methodology, N. W.; software, N. W.; validation, H. W.; data curation, Z. P.; writing-original draft preparation, N. W., and Z. P.; writing- review and editing, H. W., and J. Z.; supervision, N. W., and W. L.; project administration, H. W.; and funding acquisition, J. Z. All authors have read and agreed to the published version of the manuscript.

Funding This work was supported by the National Key Research and Development Program of China (no. 2022YFF1100203) and the collaborative innovation center of Food Safety and Quality Control in Jiangsu Province.

Data Availability No datasets were generated or analysed during the current study.

Declarations

Ethical Approval The animal experiment was approved by Jiangnan University's Animal Ethics Committee (JN. NO20230915c1441125 [400]), adhering to Chinese and international animal welfare standards. All animal experiments complied with the ARRIVE guidelines and were carried out by the U.K. Animals (Scientific Procedures) Act, 1986, and the National Research Council's Guide for the Care and Use of Laboratory Animals.

Competing Interests The authors declare no competing interests.

References

1. Mousavi T, Nikfar S, Abdollahi M (2022) The pharmacotherapeutic management of duodenal and gastric ulcers. Expert Opin Pharmacother 23(1):63–89
2. Zhu C, Zhao L, Zhao J et al (2020) Sini San ameliorates duodenal mucosal barrier injury and low-grade inflammation via the CRF pathway in a rat model of functional dyspepsia. Int J Mol Med 45(1):53–60
3. Al Nabhani Z, Berrebi D, Martinez-Vinson C et al (2020) Nod2 protects the gut from experimental colitis spreading to small intestine. J Crohns Colitis 14(5):669–679
4. De Brito BB, Da Silva FAF, Soares AS et al (2019) Pathogenesis and clinical management of Helicobacter pylori gastric infection. World J Gastroenterol 25(37):5578–5589
5. Lee SP, Lee J, Kae SH et al (2021) Effect of nonsteroidal anti-inflammatory agents on small intestinal injuries as evaluated by capsule endoscopy. Dig Dis Sci 66(8):2724–2731
6. Alam S, Ikram M, Aslam R (2019) Global incidence and prevalence of peptic ulcer disease: a systematic review study. Indo Am J Pharm Sci 6(6):11267–11273
7. Ren Z, Pan LL, Huang Y et al (2021) Gut microbiota-CRAMP axis shapes intestinal barrier function and immune responses in dietary gluten-induced enteropathy. EMBO Mol Med 13(8):e14059
8. Passali M, Josefsen K, Frederiksen JL et al (2020) Current evidence on the efficacy of gluten-free diets in multiple sclerosis, psoriasis, type 1 diabetes and autoimmune thyroid diseases. Nutrients 12(8):2316
9. Wang Y, Zhao L, Gao L et al (2021) Health policy and public health implications of obesity in China. Lancet Diabetes Endocrinol 9(7):446–461
10. Sun X, Yan AF, Shi Z et al (2022) Health consequences of obesity and projected future obesity health burden in China. Obesity (Silver Spring) 30(9):1724–1751
11. Haneishi Y, Treppiccione L, Maurano F et al (2024) High fat diet-wheat gliadin interaction and its implication for obesity and celiac disease onset: in vivo studies. Mol Nutr Food Res 68(9):e2300779
12. Freire RH, Fernandes LR, Silva RB et al (2016) Wheat gluten intake increases weight gain and adiposity associated with reduced thermogenesis and energy expenditure in an animal model of obesity. Int J Obes 40(3):479–486
13. Aguilar EC, Navia-Pelaez JM, Fernandes-Braga W et al (2020) Gluten exacerbates atherosclerotic plaque formation in ApoE-/- mice with diet-induced obesity. Nutrition:75–76. https://doi.org/10.1016/j.nut.2019.110658
14. Aguilar EC, Fernandes-Braga W, Leocadio PCL et al (2023) Dietary gluten worsens hepatic steatosis by increasing inflammation and oxidative stress in ApoE-/- mice fed a high-fat diet. Food Funct 14(7):3332–3347
15. Haro C, Guzman-Lopez MH, Marin-Sanz M et al (2022) Consumption of tritordeum bread reduces immunogenic gluten intake without altering the gut microbiota. Foods 11(10):1–17
16. Iversen KN, Carlsson F, Andersson A et al (2021) A hypocaloric diet rich in high fiber rye foods causes greater reduction in body weight and body fat than a diet rich in refined wheat: a parallel randomized controlled trial in adults with overweight and obesity (the RyeWeight study). Clin Nutr ESPEN 45:155–169
17. Kulkarni A, Patel S, Khanna D et al (2021) Current pharmacological approaches and potential future therapies for Celiac disease. Eur J Pharmacol 909:174434
18. Norouzbeigi S, Vahid-Dastjerdi L, Yekta R et al (2020) Celiac therapy by administration of probiotics in food products: a review. Curr Opin Food Sci 32:58–66
19. Laparra JM, Olivares M, Gallina O et al (2012) Bifidobacterium longum CECT 7347 modulates immune responses in a gliadin-induced enteropathy animal model. PLoS ONE 7(2):e30744
20. Herran AR, Perez-Andres J, Caminero A et al (2017) Gluten-degrading bacteria are present in the human small intestine of healthy volunteers and celiac patients. Res Microbiol 168(7):673–684
21. Pan T, Pei Z, Fang Z et al (2023) Uncovering the specificity and predictability of tryptophan metabolism in lactic acid bacteria with genomics and metabolomics. Front Cell Infect Microbiol 13:1154346
22. Yong CC, Sakurai T, Kaneko H et al (2024) Human gut-associated Bifidobacterium species salvage exogenous indole, a uremic toxin precursor, to synthesize indole-3-lactic acid via tryptophan. Gut Microbes 16(1):2347728
23. Fang Z, Pan T, Li L et al (2022) Bifidobacterium longum mediated tryptophan metabolism to improve atopic dermatitis via the gut-skin axis. Gut Microbes 14(1):2044723
24. Wang H, He Y, Dang D et al (2024) Gut microbiota-derived tryptophan metabolites alleviate allergic asthma inflammation in ovalbumin-induced mice. Foods 13(9).https://doi.org/10.3390/foods13091336
25. Giorgi A, Cerrone R, Capobianco D et al (2020) A probiotic preparation hydrolyzes gliadin and protects intestinal cells from the toxicity of pro-inflammatory peptides. Nutrients 12(2):495
26. Sharma K, Bhawanani S, Sharma D et al (2022) Selection of indigenous Lacticaseibacillus paracasei CD 4 for production of gluten-free traditional fermented product Bhaturu. Food Biotechnol 36(1):76–91
27. Tian N, Wei G, Schuppan D et al (2014) Effect of Rothia mucilaginosa enzymes on gliadin (gluten) structure, deamidation, and immunogenic epitopes relevant to celiac disease. Am J Physiol Gastrointest Liver Physiol 307(8):G769–G776
28. Zhang L, Andersen D, Roager HM et al (2017) Effects of gliadin consumption on the intestinal microbiota and metabolic homeostasis in mice fed a high-fat diet. Sci Rep 7:44613

29. Hu W, Gao W, Liu Z et al (2022) Specific strains of Faecalibacterium prausnitzii ameliorate nonalcoholic fatty liver disease in mice in association with gut microbiota regulation. Nutrients 14(14). https://doi.org/10.3390/nu14142945
30. Liao J, Liu Y, Pei Z et al (2023) Clostridium butyricum reduces obesity in a butyrate-independent way. Microorganisms 11(5). https://doi.org/10.3390/microorganisms11051292
31. Wang N, Zhang QH, Zhang L et al (2024) Characteristics of dietary patterns, and serum metabolites during the low-gluten diet among Chinese young adults. Food Biosci 61. https://doi.org/10.1016/j.fbio.2024.104829
32. Wemheuer F, Taylor JA, Daniel R et al (2020) Tax4Fun2: prediction of habitat-specific functional profiles and functional redundancy based on 16S rRNA gene sequences. Environ Microbiome 15(1):11
33. Wang G, Fan Y, Zhang G et al (2024) Microbiota-derived indoles alleviate intestinal inflammation and modulate microbiome by microbial cross-feeding. Microbiome 12(1):59
34. Martin-Masot R, Mota-Martorell N, Jove M et al (2020) Alterations in one-carbon metabolism in celiac disease. Nutrients 12(12):1–14
35. Caminero A, Nistal E, Herrán AR et al (2014) Gluten metabolism in humans [M]. 157–170. https://doi.org/10.1016/B978-0-12-401716-0.00013-1
36. Sakurai T, Yamada A, Hashikura N et al (2018) Degradation of food-derived opioid peptides by bifidobacteria. Benef Microbes 9(4):675–682
37. Nandhra GK, Mark EB, Di Tanna GL et al (2020) Normative values for region-specific colonic and gastrointestinal transit times in 111 healthy volunteers using the 3D-Transit electromagnet tracking system: influence of age, gender, and body mass index. Neurogastroenterol Motil 32(2):e13734
38. Fan S, Chen S, Lin L (2023) Research progress of gut microbiota and obesity caused by high-fat diet. Front Cell Infect Microbiol 13:1139800
39. Fasano A, Matera M (2024) Probiotics to prevent celiac disease and inflammatory bowel diseases. Adv Exp Med Biol 1449:95–111
40. Hansen LBS, Roager HM, Sondertoft NB et al (2018) A low-gluten diet induces changes in the intestinal microbiome of healthy Danish adults. Nat Commun 9(1):4630
41. Zong G, Lebwohl B, Hu FB et al (2018) Gluten intake and risk of type 2 diabetes in three large prospective cohort studies of US men and women. Diabetologia 61(10):2164–2173
42. Rune I, Rolin B, Larsen C et al (2016) Modulating the gut microbiota improves glucose tolerance, lipoprotein profile and atherosclerotic plaque development in ApoE-deficient mice. PLoS ONE 11(1):e0146439
43. Przemioslo RT, Kontakou M, Nobili V et al (1994) Raised pro-inflammatory cytokines interleukin 6 and tumour necrosis factor alpha in coeliac disease mucosa detected by immunohistochemistry. 35(10):1398. https://doi.org/10.1136/gut.35.10.1398
44. Auricchio R, Calabrese I, Galatola M et al (2022) Gluten consumption and inflammation affect the development of celiac disease in at-risk children. Sci Rep 12(1):5396
45. Laparra JM, Sanz Y (2010) Bifidobacteria inhibit the inflammatory response induced by gliadins in intestinal epithelial cells via modifications of toxic peptide generation during digestion. J Cell Biochem 109(4):801–807
46. Olivares M, Castillejo G, Varea V et al (2014) Double-blind, randomised, placebo-controlled intervention trial to evaluate the effects of Bifidobacterium longum CECT 7347 in children with newly diagnosed coeliac disease. Br J Nutr 112(1):30–40
47. Wlodarska M, Luo C, Kolde R et al (2017) Indoleacrylic acid produced by commensal Peptostreptococcus species suppresses inflammation. Cell Host Microbe 22(1):25-37 e6
48. Zhang X, Shi L, Wang N et al (2023) Gut bacterial indole-3-acetic acid induced immune promotion mediates preventive effects of Fu brick tea polyphenols on experimental colitis. J Agric Food Chem 71(2):1201–1213
49. Caminero A, Herrán AR, Nistal E et al (2014) Diversity of the cultivable human gut microbiome involved in gluten metabolism: isolation of microorganisms with potential interest for coeliac disease. FEMS Microbiol Ecol 88(2):309–319
50. Sanchez E, Laparra JM, Sanz Y (2012) Discerning the role of Bacteroides fragilis in celiac disease pathogenesis. Appl Environ Microbiol 78(18):6507–6515
51. Jacob T, Sindhu S, Hasan A et al (2024) Soybean oil-based HFD induces gut dysbiosis that leads to steatosis, hepatic inflammation and insulin resistance in mice. Front Microbiol 15:1407258
52. Yu T, Xie Y, Wang Z et al (2024) Quercetin ameliorates celiac-related intestinal inflammation caused by wheat gluten through modulating oxidative stress, Th1/Th2/Treg balance, and intestinal microflora structure. Food Funct 2024(18):15
53. Carnicero-Mayo Y, Saenz De Miera LE, Ferrero MA et al (2024) Modeling dynamics of human gut microbiota derived from gluten metabolism: obtention, maintenance and characterization of complex microbial communities. Int J Mol Sci 25(7). https://doi.org/10.3390/ijms25074013
54. Khan A, Li S, Han H et al (2023) A gluten degrading probiotic Bacillus subtilis LZU-GM relieve adverse effect of gluten additive food and balances gut microbiota in mice. Food Res Int 170:112960
55. Feng J, Ma H, Huang Y et al (2022) Ruminococcaceae_UCG-013 promotes obesity resistance in mice. Biomedicines 10(12). https://doi.org/10.3390/biomedicines10123272
56. Lee H, An J, Kim J et al (2022) A novel Bacterium, Butyricimonas virosa, preventing HFD-induced diabetes and metabolic disorders in mice via GLP-1 receptor. Front Microbiol 13:858192
57. Kwiecinska-Pirog J, Chomont K, Fydrych D et al (2024) How xylitol, gluten, and lactose change human gut microbiota Escherichia coli and Lactobacillus rhamnosus GG biofilm. Nutrition 124:112446
58. Xie Q, Liu C, Fu W et al (2023) Combination of gut microbial features and the proteomic pattern revealed changes in specific intestinal luminal factors and mechanisms of their regulation of gluten allergy. J Agric Food Chem 71(33):12558–12573
59. Wei C, Xu T, Geng Y et al (2024) High-fat diet disrupts the gut microbiome, leading to inflammation, damage to tight junctions, and apoptosis and necrosis in Nyctereutes procyonoides intestines. Microbiol Spectr 12(4). https://doi.org/10.1128/spectrum.04182-23
60. Bibbo S, Abbondio M, Sau R et al (2020) Fecal microbiota signatures in celiac disease patients with poly-autoimmunity. Front Cell Infect Microbiol 10:349